Raytheon

PRECIPITABLE WATER

VISIBLE/INFRARED IMAGER/RADIOMETER SUITE ALGORITHM THEORETICAL BASIS DOCUMENT

Version 4: May 2001

Allen Huang
Weather Or Knot

Shawn W. Miller
Donglian Sun

RAYTHEON COMPANY
Information Technology and Scientific Services
4400 Forbes Boulevard
Lanham, MD 20706

SRBS Document #: Y3251

EDR: PRECIPITABLE WATER

Doc No: Y3251

Version: 4

Revision: 0

	Function	Name	Signature	Date
Prepared by	EDR Developer	A. HUANG		5/3/01
Approved by	Reviewer	R. SLONAKER		5/13/01
Approved by	Relevant Lead	R. SIKORSKI		5/13/01
Approved by	Chief Scientist	S. MILLER		5/14/01
Released by	Algorithm Lead	P. KEALY		5/15/01

TABLE OF CONTENTS

Page

LIST OF FIGURES

Page

LIST OF TABLES

Page

GLOSSARY OF ACRONYMS

AOT	Aerosol Optical Thickness
ARVI	Atmospherically Resistant Vegetation Index
ATB	Algorithm Theoretical Basis
ATBD	Algorithm Theoretical Basis Document
AVHRR	Advanced Very High Resolution Radiometer
BBR	Band-to-Band Registration
BRDF	Bidirectional Reflectance Distribution Function
BRF	Bidirectional Reflectance Factor
CMIS	Conical Scanning Microwave Imager/Sounder
CrIS	Cross-track Infrared Sounder
DN	Digital Number
DoD	Department of Defense
DISORT	Discrete Ordinate Radiative Transfer Model
EDR	Environmental Data Record
EOS	Earth Observing System
FPAR	Fraction of absorbed Photosynthetically Active Radiation
GIFOV	Ground Instantaneous Field of View
GRASSI	Green Reflectance-based Atmospheric and Soil-corrected Surface Index
GSD	Ground Sampling Distance
HCS	Horizontal Cell Size
HITRAN	High Resolution Transmission Model
HSR	Horizontal Spatial Resolution
IBR	In Band Response
IFOV	Instantaneous Field of View
IPO	Integrated Program Office
IVI	Integrated Vegetation Index
JHU	Johns Hopkins University
LAI	Leaf Area Index
LBL	Line by Line
LLLS	Low Level Light Sensor
LUT	Look-up Table
MODIS	Moderate Resolution Imaging Spectroradiometer
MODTRAN	Moderate Resolution Transmission Model
MISR	Multi-Angle Imaging Spectroradiometer
MTF	Modulation Transfer Function
MVI	MODIS Vegetation Index
NASA	National Aeronautics and Space Administration
NASA/GSFC	NASA Goddard Space Flight Center
NASA/JPL	NASA Jet Propulsion Laboratory
NDVI	Normalized Difference Vegetation Index

NedL	Noise Equivalent Delta Radiance
NIR	Near Infrared
NOAA	National Oceanic and Atmospheric Administration
NPOESS	National Polar-orbiting Operational Environmental Satellite System
NPP	Net Primary Productivity
OLS	Operational Linescan System
OMPS	Ozone Mapping Profiling Suite
ONVI	Off-Nadir Vegetation Index
OOBL	Out of Band Leakage
OOBR	Out of Band Response
PAR	Photosynthetically Active Radiation
PDR	Preliminary Design Review
PSF	Point Spread Function
PSN	Net Photosynthesis
RDR	Raw Data Record
RSC	Raytheon Systems Company
SARVI	Soil-corrected and Atmospherically Resistant Vegetation Index
SARVI2	Modified Soil corrected Atmospherically Resistant Vegetation Index
SAVI	Soil Adjusted Vegetation Index
SBRS	Santa Barbara Remote Sensing
SNR	Signal-to-Noise Ratio
SRD	Sensor Requirements Document
TIROS	Television Infrared Observation Satellite
TM	Thematic Mapper
TOA	Top of Atmosphere
TOC	Top of Canopy
USGS	United States Geological Survey
VI1	Primary Vegetation Index
VIIRS	Visible/Infrared Imager/Radiometer Suite
VIST	Vegetation Index/Surface Type EDR
VVI	VIIRS Vegetation Index

ABSTRACT

Precipitable Water is one of more than two dozen environmental data records (EDRs) explicitly required as products to be derived from the Visible/Infrared Imager/Radiometer Suite (VIIRS) sensor slated to fly onboard the National Polar-orbiting Operational Environmental Satellite System (NPOESS), which is scheduled for launch in the late 2000's. The requirements for the VIIRS EDRs are described in detail in the VIIRS Sensor Requirements Document (SRD). These requirements form the foundation from which both the algorithms and the sensor are designed and built. A revised version of the SRD was released in November 1999, detailing a set of new requirements targeted toward the NPOESS Preparatory Program (NPP), a National Aeronautics and Space Administration (NASA) endeavor to build upon the MODIS heritage beginning in 2005. The Precipitable Water EDR was added to the VIIRS SRD at that time

The Precipitable Water EDR will be retrieved globally, both day and night, and under both clear and cloudy conditions. Under cloudy conditions, the retrievals will only include precipitable water above the clouds. The baseline algorithm for the Precipitable Water EDR is a brightness temperature regression approach similar to the traditional methods for deriving sea surface temperature (SST). Data from five bands will be used in conjunction with solar/viewing geometry and surface pressure to arrive at the final product, which will provide measurements of column water vapor at high spatial resolution to complement the equivalent microwave-derived product in the NPOESS suite of EDRs.

This document includes a thorough description of the established behavior of the Precipitable Water EDR. . Simulated trade-off study which account for the effects of measurement noise, forward model error, atmospheric state uncertainties, aerosol contamination, and sub-visible cirrus cloud is documented. VIIRS spectral measurements characteristics related to precipitable water, historical development of retrieving precipitable water, and detailed mathematical description of the proposed non-linear regression retrieval algorithm are also discussed. These simulations have permitted the construction and characterization of a robust package of environmental products which will build upon the existing MODIS heritage.

1.0 INTRODUCTION

1.1 PURPOSE

This algorithm theoretical basis document (ATBD) describes the algorithms used to retrieve the Precipitable Water Environmental Data Record (EDR) for the Visible/Infrared Imager/Radiometer Suite (VIIRS). The primary purpose of this ATBD is to establish guidelines for the production of the Precipitable Water EDR. This document will describe the required inputs, a theoretical description of the algorithms, the sources and magnitudes of the errors involved, practical considerations for post-launch implementation, and the assumptions and limitations associated with the products.

1.2 SCOPE

This document covers the algorithm theoretical basis (ATB) for the operational retrieval of the Precipitable Water EDR. Any derived products beyond the generation of this EDR will not be discussed. The exact structure of the algorithm for the Precipitable Water EDR may change during the developmental phase of this experiment; this document will be revised accordingly to match those changes. Only the algorithm that will be implemented for routine operational processing will be preserved in the final release of this document.

Section 1 describes the purpose and scope of this document; it also includes a listing of VIIRS documents that will be cited in the following sections. Section 2 provides a brief overview of the motivation for the Precipitable Water algorithm, including the objectives of the retrievals, the currently designed VIIRS instrument characteristics, and the strategy for retrieval of the Precipitable Water EDR. Section 3 contains the essence of this document – a complete description of the Precipitable Water EDR. Consideration is given to the overall structure, the required inputs, a theoretical description of the products, assessment of the error budget, results of ongoing sensitivity studies, practical implementation issues, validation, and the algorithm development schedule. Section 4 provides an overview of the constraints, assumptions and limitations associated with the Precipitable Water EDR, and Section 5 contains a listing of references cited throughout the course of this document.

1.3 VIIRS DOCUMENTS

Reference to VIIRS documents within this ATBD will be indicated by an italicized number in brackets, e.g., *[V-1]*.

[V-1] VIIRS Surface Type ATBD.

[V-3] VIIRS Geolocation ATBD.

[V-4] VIIRS Calibration/Validation Plan.

[V-5] VIIRS Cloud Mask ATBD.

[V-6] VIIRS Surface Reflectance ATBD.

[V-7] VIIRS Aerosol Optical Thickness ATBD.

1.4 REVISIONS

This is the second working version of this document, version 4. It is dated May 2001. There were no versions numbered 1.0 or 2.0; the current version number has been selected to match the delivery of the previously existing VIIRS EDR ATBDs, which underwent two previous version releases.

2.0 EXPERIMENT OVERVIEW

2.1 OBJECTIVES OF PRECIPITABLE WATER RETRIEVALS

The overall scientific objective of the VIIRS Precipitable Water EDR is to provide improved, high-spatial-resolution, global precipitable water fields. Precipitable water is defined as the total equivalent water in a vertical column of the atmosphere per unit cross-sectional area. The Precipitable Water EDR is crucial for our understanding of the hydrological cycle, aerosol-cloud interactions, energy budget, and climate. Precipitable water is also an important parameter for deriving other VIIRS EDRs, such as sea surface and land surface temperature. Accurate knowledge about precipitable water will enable improved SST and LST EDRs, as all the infrared VIIRS spectral measurements are strongly affected by water vapor absorption.

2.2 INSTRUMENT CHARACTERISTICS

The VIIRS instrument will now be briefly described to clarify the context of the descriptions of the Precipitable Water EDR presented in this document. VIIRS can be pictured as a convergence of three existing sensors, two of which have seen extensive operational use at this writing.

The Operational Linescan System (OLS) is the operational visible/infrared scanner for the Department of Defense (DoD). Its unique strengths are controlled growth in spatial resolution through rotation of the ground instantaneous field of view (GIFOV) and the existence of a low-level light sensor (LLLS) capable of detecting visible radiation at night. OLS has primarily served as a data source for manual analysis of imagery. The Advanced Very High Resolution Radiometer (AVHRR) is the operational visible/infrared sensor flown on the National Oceanic and Atmospheric Administration (NOAA) Television Infrared Observation Satellite (TIROS-N) series of satellites (Planet, 1988). Its unique strengths are low operational and production cost and the presence of five spectral channels that can be used in a wide number of combinations to produce operational and research products. In December 1999, the National Aeronautics and Space Administration (NASA) launched the Earth Observing System (EOS) morning satellite, *Terra*, which includes the Moderate Resolution Imaging Spectroradiometer (MODIS). This sensor possesses an unprecedented array of thirty-two spectral bands at resolutions ranging from 250 m to 1 km at nadir, allowing for unparalleled accuracy in a wide range of satellite-based environmental measurements.

VIIRS will reside on a platform of the National Polar-orbiting Operational Environmental Satellite System (NPOESS) series of satellites. It is intended to be the product of a convergence between DoD, NOAA and NASA in the form of a single visible/infrared sensor capable of satisfying the needs of all three communities, as well as the research community beyond. As such, VIIRS will require three key attributes: high spatial resolution with controlled growth off nadir, minimal production and operational cost, and a large number of spectral bands to satisfy the requirements for generating accurate operational and scientific products.

Figure 1 illustrates the design concept for VIIRS, designed and built by Raytheon Santa Barbara Remote Sensing (SBRS). At its heart is a rotating telescope scanning mechanism that minimizes the effects of solar impingement and scattered light. Calibration is performed onboard using a solar diffuser for short wavelengths and a V-groove blackbody source and deep space view for thermal wavelengths. A solar diffuser stability monitor (SDSM) is also included to track the

performance of the solar diffuser. The nominal altitude for NPOESS will be 833 km. The VIIRS scan will extend to 56 degrees on either side of nadir.

The VIIRS SRD places explicit requirements on spatial resolution for the Imagery EDR. Specifically, the horizontal spatial resolution (HSR) of bands used to meet threshold Imagery EDR requirements must be no greater than 400 m at nadir and 800 m at the edge of the scan. This led to the development of a unique scanning approach which optimizes both spatial resolution and signal to noise ratio (SNR) across the scan. The concept is summarized in Figure 2 for the imagery bands; the nested lower resolution radiometric bands follow the same paradigm at exactly twice the size. The VIIRS detectors are rectangular, with the smaller dimension projecting along the scan. At nadir, three detector footprints are aggregated to form a single VIIRS "pixel." Moving along the scan away from nadir, the detector footprints become larger both along track and along scan, due to geometric effects and the curvature of the Earth. The effects are much larger along scan. At around 32 degrees in scan angle, the aggregation scheme is changed from 3x1 to 2x1. A similar switch from 2x1 to 1x1 aggregation occurs at 48 degrees. The VIIRS scan consequently exhibits a pixel growth factor of only 2 both along track and along scan, compared with a growth factor of 6 along scan which would be realized without the use of the aggregation scheme. Figure 3 illustrates the benefits of the aggregation scheme for spatial resolution.

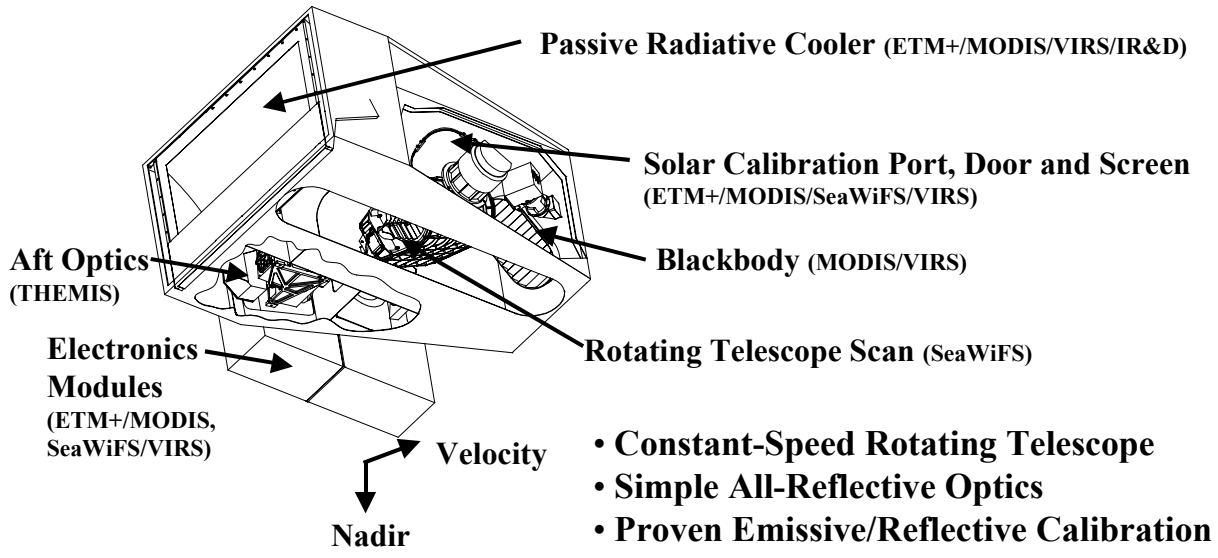

Figure 1. Summary of VIIRS design concepts and heritage.

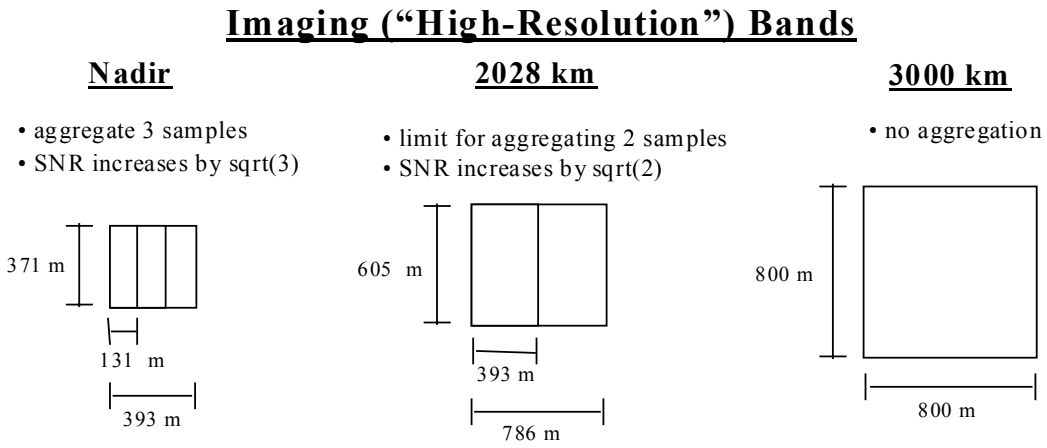

Figure 2. VIIRS detector footprint aggregation scheme for building "pixels."

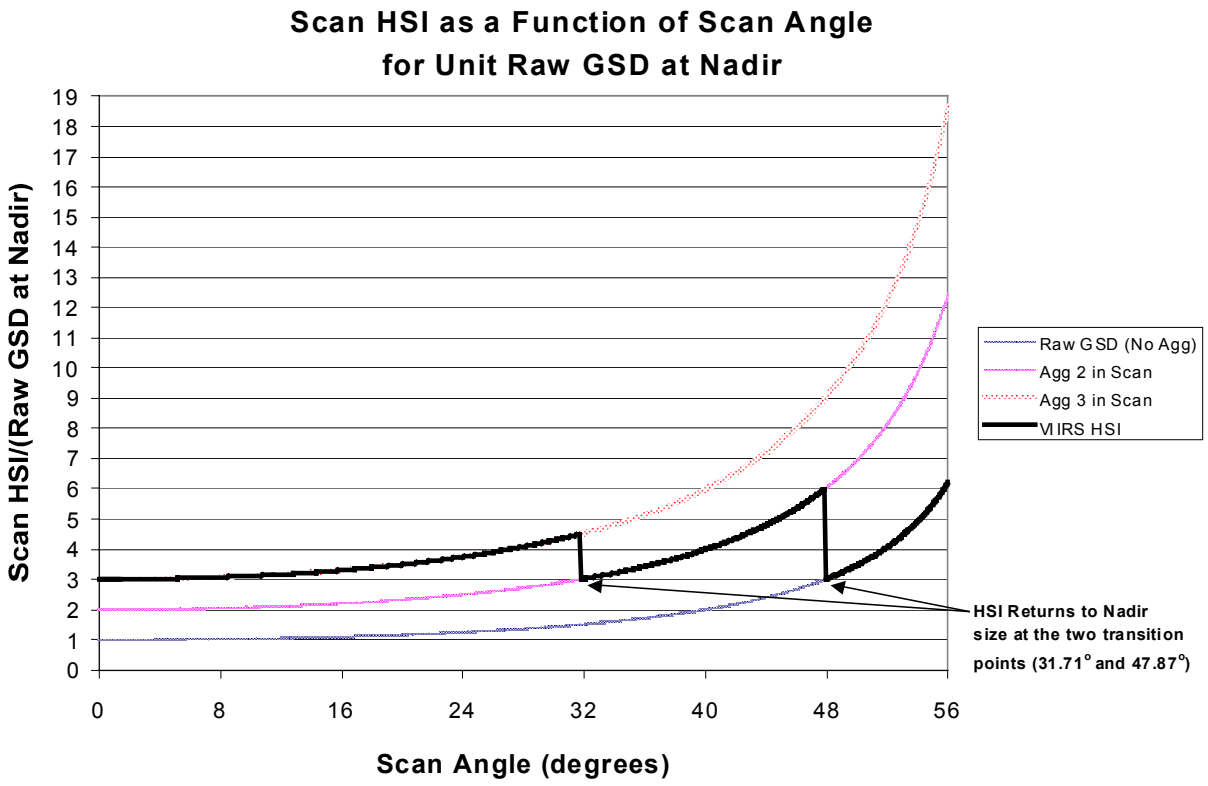

Figure 3. Benefits of VIIRS aggregation scheme in reducing pixel growth at edge of scan.

The VIIRS baseline performance is summarized in Table 1 and Table 2 for low and high radiances, respectively. The low radiance numbers for the middle and long-wave infrared bands are more relevant to Precipitable Water retrievals in general. The exact values of these numbers can be expected to change through the design and fabrication stages for VIIRS; each release of this document will reflect the latest numbers at the time of its release, however minor discrepancies may develop if the document is being read a significant amount of time since the most recent release. The positioning of the VIIRS spectral bands is summarized in Figure 4 through Figure 7.

VIIRS Baseline Performance and Specifications													20-Mar-00															
Q=W/m^2/sr/μm															LOW RADIANCE													
			GSD (m)														3x1 Agg		2x1 Agg		Native		Native Spec					
Band	Wave (μm)	BW (μm)	Nadir		31.71°		43.60°		47.87°		55.84°		Gain/ TDI	L/T typ Q/K	L/T max Q/K	SNR @Ltyp (e-/e-)	NEDT @Ttyp (K)	SNR @Ltyp (e-/e-)	NEDT @Ttyp (K)	SNR @Ltyp (e-/e-)	NEDT @Ttyp (K)	SNR @Ltyp (e-/e-)	NEDT @Ttyp (K)	SNR Margin (%)	Solar Irr over π Q	Driving EDR (Radiometric)
			Trk	Scn	Trk	Scn	Trk	Scn	Trk	Scn	Trk	Scn																
DNB	0.700	0.4000	742	742	742	742	742	742	742	742	742	742	variable	6.7E-05	500	n/a	n/a	n/a	n/a	**8.0**	n/a	**6.0**	n/a	33.3%	364.9	Imagery (Clouds)
ch2w2	0.412	0.0200	742	262	895	393	1094	617	1213	786	1600	1600	D/1	44.9	135	752.3	n/a	614.2	n/a	**434.3**	n/a	**352.0**	n/a	23.4%	544.4	Ocean Color
2	0.445	0.0180	742	262	895	393	1094	617	1213	786	1600	1600	D/1	40.0	127	925.0	n/a	755.3	n/a	**534.1**	n/a	**337.8**	n/a	58.1%	610.1	Ocean Color
ch8	0.488	0.0200	742	262	895	393	1094	617	1213	786	1600	1600	D/1	32.0	107	987.1	n/a	806.0	n/a	**569.9**	n/a	**310.6**	n/a	83.5%	623.6	Ocean Color
4	0.555	0.0200	742	262	895	393	1094	617	1213	786	1600	1600	D/1	21.0	78	846.2	n/a	690.9	n/a	**488.6**	n/a	**257.1**	n/a	90.0%	592.4	Ocean Color
5i	0.645	0.0500	371	131	448	196	547	309	606	393	800	800	S/1	n/a	n/a	n/a	n/a	n/a	n/a	n/a	n/a	n/a	n/a	n/a	n/a	n/a
oc2	0.672	0.0200	742	262	895	393	1094	617	1213	786	1600	1600	D/1	10.0	59	584.7	n/a	477.4	n/a	**337.6**	n/a	**242.1**	n/a	39.4%	485.3	Ocean Color
oc3	0.751	0.0150	742	262	895	393	1094	617	1213	786	1600	1600	S/1	9.6	41	481.1	n/a	392.8	n/a	**277.8**	n/a	**199.1**	n/a	39.5%	402.3	Ocean Color
6i	0.865	0.0390	371	131	448	196	547	309	606	393	800	800	S/1	n/a	n/a	n/a	n/a	n/a	n/a	n/a	n/a	n/a	n/a	n/a	n/a	n/a
6r	0.865	0.0390	742	262	895	393	1094	617	1213	786	1600	1600	D/1	6.4	29	823.4	n/a	672.3	n/a	**475.4**	n/a	**215.3**	n/a	120.8%	310.2	Ocean Color
cd1	1.240	0.0200	742	262	895	393	1094	617	1213	786	1600	1600	S/1	n/a	n/a	n/a	n/a	n/a	n/a	n/a	n/a	n/a	n/a	n/a	n/a	n/a
7	1.378	0.0150	742	262	895	393	1094	617	1213	786	1600	1600	S/1	n/a	n/a	n/a	n/a	n/a	n/a	n/a	n/a	n/a	n/a	n/a	n/a	n/a
8i	1.610	0.0600	371	131	448	196	547	309	606	393	800	800	S/1	n/a	n/a	n/a	n/a	n/a	n/a	n/a	n/a	n/a	n/a	n/a	n/a	n/a
8r	1.610	0.0600	742	262	895	393	1094	617	1213	786	1600	1600	S/1	0.42	16.3	54.0	n/a	44.1	n/a	**31.2**	n/a	**14.6**	n/a	113.5%	78.1	Aerosols (Ocean)
9	2.250	0.0500	742	262	895	393	1094	617	1213	786	1600	1600	S/1	0.12	5.6	24.1	n/a	19.7	n/a	**13.9**	n/a	**10.0**	n/a	39.3%	24.0	Aerosols (Ocean)
10iw	3.740	0.3800	371	131	448	196	547	309	606	393	800	800	S/1	270	353	17.1	1.108	14.0	1.356	**9.9**	1.918	**7.8**	2.436	27.0%	n/a	Imagery (Clouds)
10r	3.700	0.1800	742	262	895	393	1094	617	1213	786	1600	1600	S/1	270	310	131.7	0.142	107.5	0.174	**76.0**	0.247	**47.3**	0.396	60.6%	n/a	Cloud Top Properties
sst2	4.050	0.1550	742	262	895	393	1094	617	1213	786	1600	1600	D/1	300	338	823.6	0.031	672.5	0.038	**475.5**	0.053	**237.7**	0.107	100.0%	n/a	SST
sst4	8.550	0.3000	742	262	895	393	1094	617	1213	786	1600	1600	S/1	270	336	1616.1	0.027	1319.5	0.033	**933.1**	0.046	**475.8**	0.091	96.1%	n/a	Cloud Optical Properties
11	10.7625	1.0000	742	262	895	393	1094	617	1213	786	1600	1600	S/1	260	310	1119.8	0.045	914.3	0.055	**646.5**	0.078	**408.7**	0.123	58.2%	n/a	Cloud Top Properties
12iw	11.450	1.9000	371	131	448	196	547	309	606	393	800	800	S/1	210	310	82.1	0.426	67.1	0.522	**47.4**	0.738	**23.3**	1.500	103.2%	n/a	Imagery (Clouds)
12r	12.0125	0.9500	742	262	895	393	1094	617	1213	786	1600	1600	S/2	270	310	1424.2	0.042	1162.8	0.052	**822.2**	0.073	**448.8**	0.134	83.2%	n/a	Cloud Cover

Table 1. VIIRS baseline performance and specifications, low radiance range.

VIIRS Baseline Performance and Specifications																												
Q=W/m^2/sr/μm															HIGH RADIANCE													
			GSD (m)														3x1 Agg		2x1 Agg		Native		Native Spec					
Band	Wave (μm)	BW (μm)	Nadir		31.71°		43.60°		47.87°		55.84°		Gain/ TDI	L/T typ Q/K	L/T max Q/K	SNR @Ltyp (e-/e-)	NEDT @Ttyp (K)	SNR @Ltyp (e-/e-)	NEDT @Ttyp (K)	SNR @Ltyp (e-/e-)	NEDT @Ttyp (K)	SNR @Ltyp (e-/e-)	NEDT @Ttyp (K)	SNR Margin (%)	Solar Irr over π Q	Driving EDR (Radiometric)
			Trk	Scn	Trk	Scn	Trk	Scn	Trk	Scn	Trk	Scn																
DNB	0.700	0.4000	742	742	742	742	742	742	742	742	742	742	variable	n/a	n/a	n/a	n/a	n/a	n/a	n/a	n/a	n/a	n/a	n/a	n/a	n/a
ch2w2	0.412	0.0200	742	262	895	393	1094	617	1213	786	1600	1600	D/1	55.0	465	867.0	n/a	707.9	n/a	**500.5**	n/a	**316.3**	n/a	58.2%	544.4	Suspended Matter
2	0.445	0.0180	742	262	895	393	1094	617	1213	786	1600	1600	D/1	55.5	469	1152.3	n/a	940.9	n/a	**665.3**	n/a	**409.8**	n/a	62.4%	610.1	Suspended Matter
ch8	0.488	0.0200	742	262	895	393	1094	617	1213	786	1600	1600	D/1	51.8	541	1357.4	n/a	1108.3	n/a	**783.7**	n/a	**414.3**	n/a	89.1%	623.6	Aerosols
4	0.555	0.0200	742	262	895	393	1094	617	1213	786	1600	1600	D/1	29.0	590	1056.5	n/a	862.6	n/a	**610.0**	n/a	**315.4**	n/a	93.4%	592.4	Suspended Matter
5i	0.645	0.0500	371	131	448	196	547	309	606	393	800	800	S/1	22.0	468	317.9	n/a	259.5	n/a	**183.5**	n/a	**130.7**	n/a	40.4%	510.9	Vegetation Index
oc2	0.672	0.0200	742	262	895	393	1094	617	1213	786	1600	1600	D/1	22.0	468	1031.6	n/a	842.3	n/a	**595.6**	n/a	**406.0**	n/a	46.7%	485.3	Aerosols
oc3	0.751	0.0150	742	262	895	393	1094	617	1213	786	1600	1600	S/1	n/a	n/a	n/a	n/a	n/a	n/a	n/a	n/a	n/a	n/a	n/a	n/a	n/a
6i	0.865	0.0390	371	131	448	196	547	309	606	393	800	800	S/1	25.0	278	418.7	n/a	341.8	n/a	**241.7**	n/a	**151.2**	n/a	59.8%	310.2	Vegetation Index
6r	0.865	0.0390	742	262	895	393	1094	617	1213	786	1600	1600	D/1	25.0	278	1989.7	n/a	1624.6	n/a	**1149**	n/a	**508.8**	n/a	125.8%	310.2	Aerosols
cd1	1.240	0.0200	742	262	895	393	1094	617	1213	786	1600	1600	S/1	5.40	95	228.2	n/a	186.3	n/a	**131.8**	n/a	**101.0**	n/a	30.5%	149.2	Cloud Optical Properties
7	1.378	0.0150	742	262	895	393	1094	617	1213	786	1600	1600	S/1	6.00	41	230.5	n/a	188.2	n/a	**133.1**	n/a	**82.7**	n/a	60.9%	114.6	Aerosols
8i	1.610	0.0600	371	131	448	196	547	309	606	393	800	800	S/1	7.3	56.7	134.5	n/a	109.8	n/a	**77.7**	n/a	**6.0**	n/a	1194%	78.1	Snow Cover/Depth
8r	1.610	0.0600	742	262	895	393	1094	617	1213	786	1600	1600	S/1	7.30	72.5	838.9	n/a	685.0	n/a	**484.3**	n/a	**342.2**	n/a	41.5%	78.1	Aerosols (Land)
9	2.250	0.0500	742	262	895	393	1094	617	1213	786	1600	1600	S/1	1.00	31.8	193.2	n/a	157.8	n/a	**111.6**	n/a	**78.9**	n/a	41.4%	24.0	Aerosols (Land)
10iw	3.740	0.3800	371	131	448	196	547	309	606	393	800	800	S/1	n/a	n/a	n/a	n/a	n/a	n/a	n/a	n/a	n/a	n/a	n/a	n/a	n/a
10r	3.700	0.1800	742	262	895	393	1094	617	1213	786	1600	1600	S/1	300	353	512.0	0.045	418.0	0.055	**295.6**	0.078	**165.3**	0.140	78.8%	n/a	SST
sst2	4.050	0.1550	742	262	895	393	1094	617	1213	786	1600	1600	D/1	335	500	2203.3	0.014	1799.0	0.018	**1272**	0.025	**15.8**	2.000	7954%	n/a	Active Fires
sst4	8.550	0.3000	742	262	895	393	1094	617	1213	786	1600	1600	S/1	n/a	n/a	n/a	n/a	n/a	n/a	n/a	n/a	n/a	n/a	n/a	n/a	n/a
11	10.7625	1.0000	742	262	895	393	1094	617	1213	786	1600	1600	S/1	300	408	2235.7	0.030	1825.4	0.036	**1291**	0.052	**950.6**	0.070	35.8%	n/a	SST
12iw	11.450	1.9000	371	131	448	196	547	309	606	393	800	800	S/1	n/a	n/a	n/a	n/a	n/a	n/a	**179.9**	n/a	**n/a**	n/a	n/a	n/a	n/a
12r	12.0125	0.9500	742	262	895	393	1094	617	1213	786	1600	1600	S/2	300	340	2234.2	0.033	1824.2	0.040	**1290**	0.057	**1024**	0.072	25.9%	n/a	SST

Table 2. VIIRS baseline performance and specifications, high radiance range.

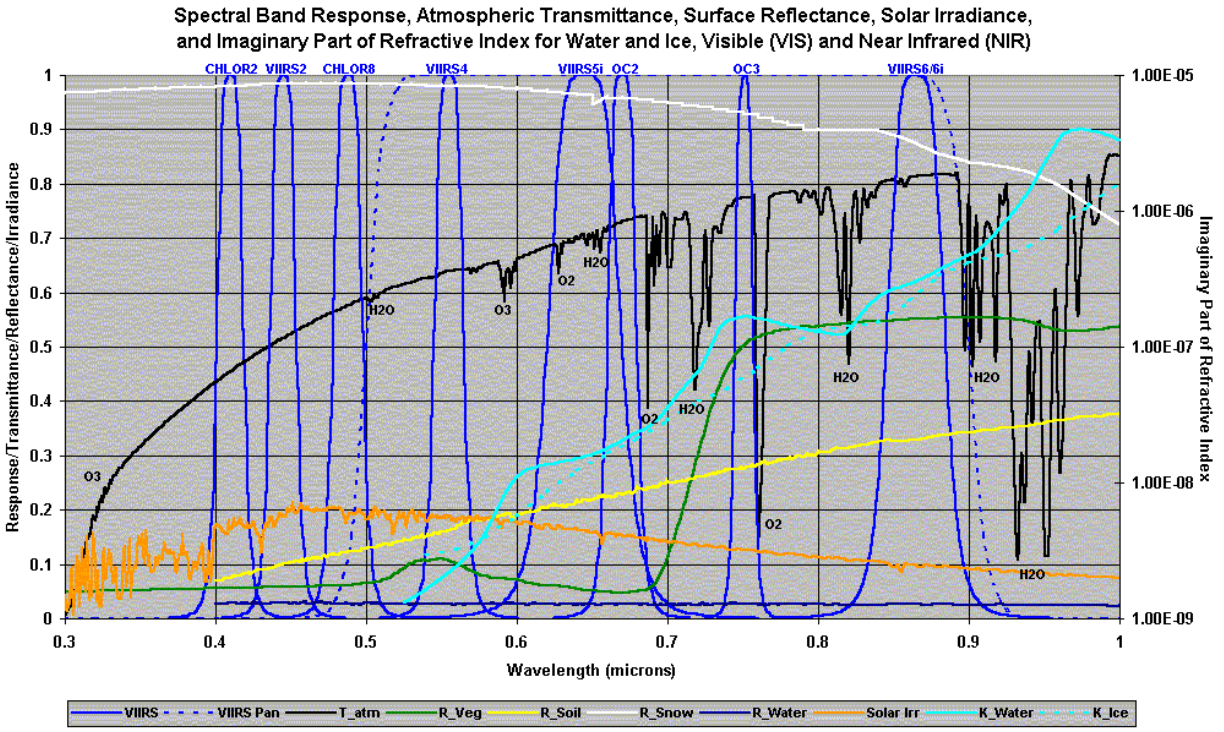

Figure 4. VIIRS spectral bands, visible and near infrared.

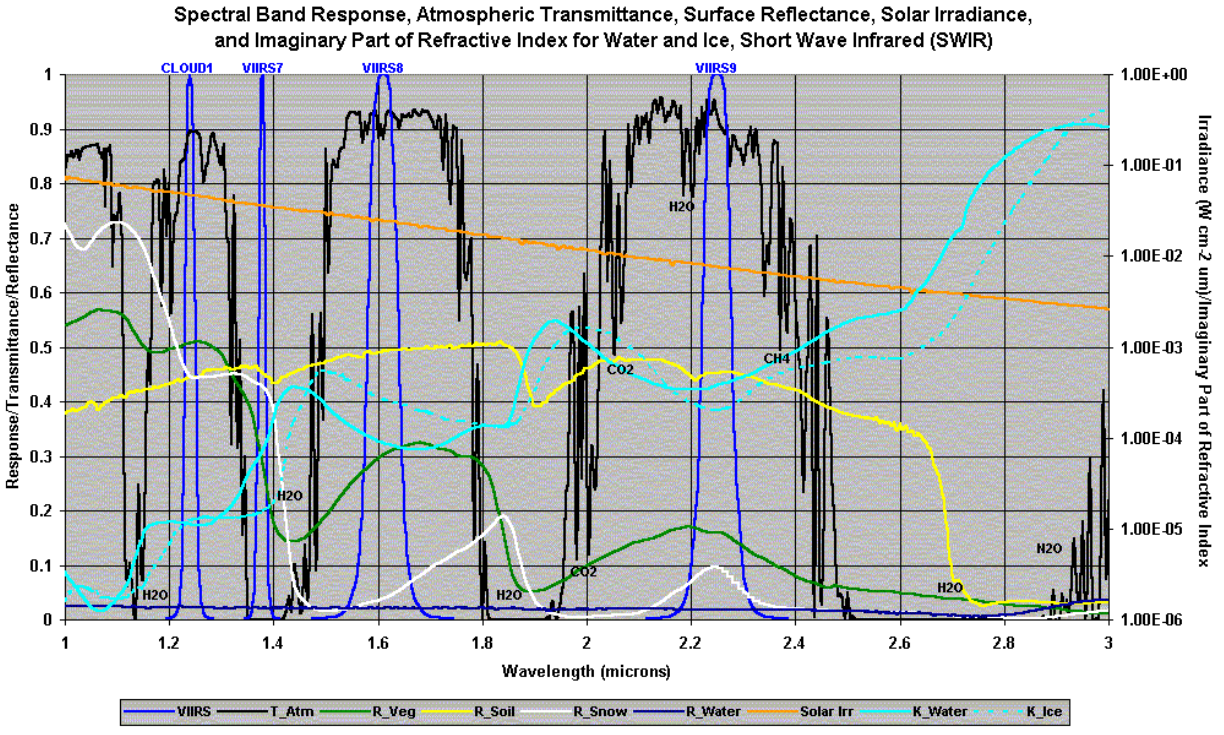

Figure 5. VIIRS spectral bands, short wave infrared.

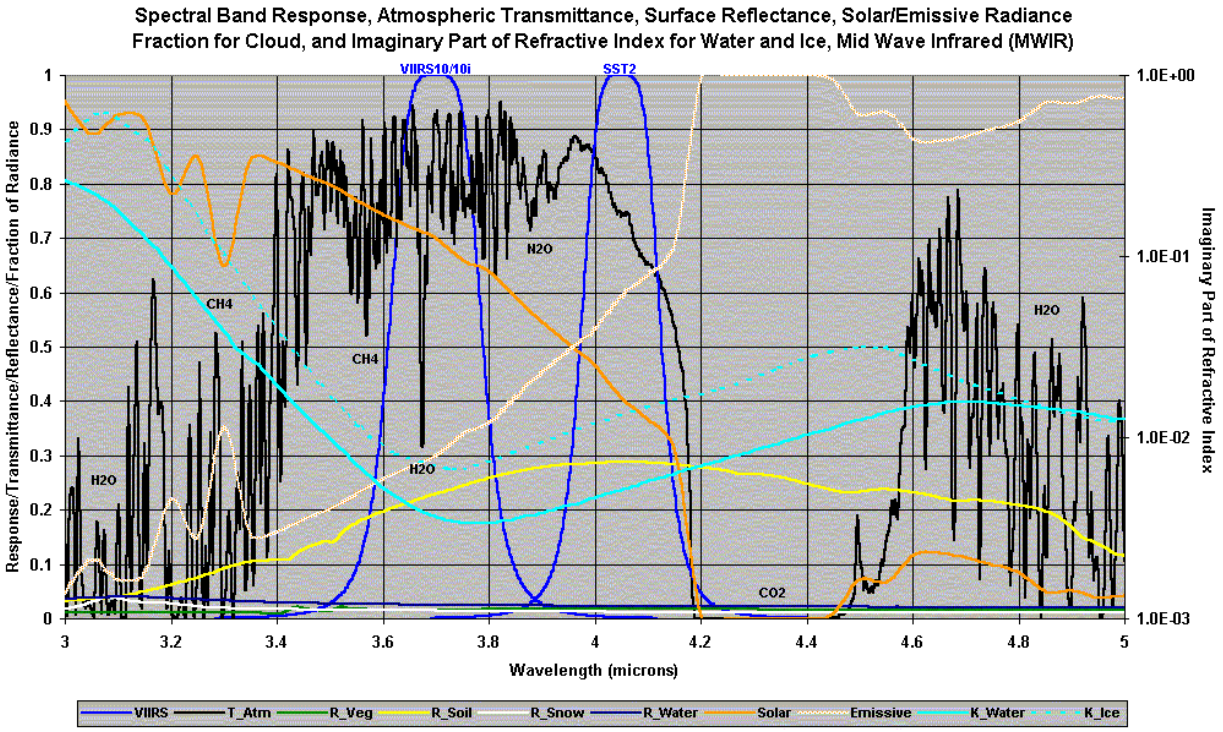

Figure 6. VIIRS spectral bands, medium wave infrared.

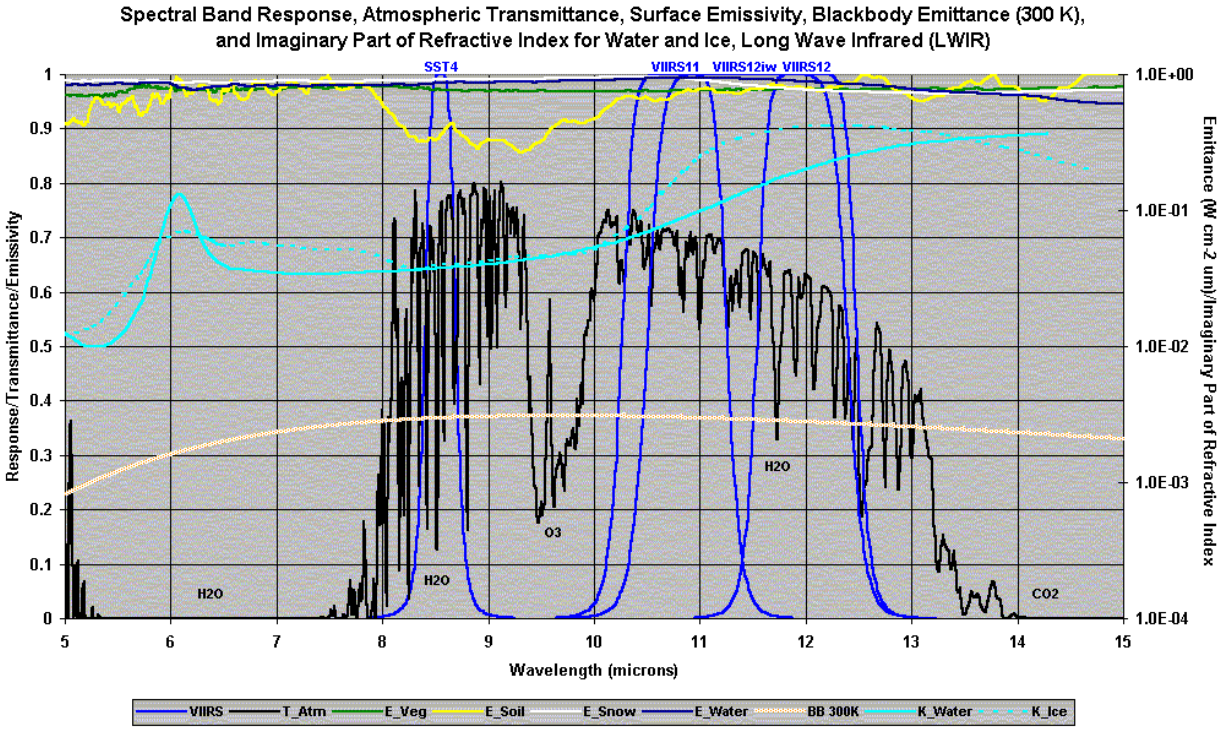

Figure 7. VIIRS spectral bands, long wave infrared.

2.3 RETRIEVAL STRATEGY

The Precipitable Water EDR is essentially a non-linear function of earth atmosphere parameters such as earth surface temperature, surface characteristics (emissivity and reflectivity), and temperature and water vapor profile conditions. VIIRS baseline infrared measurements are designed to be sensitive to all these elements that govern the Precipitable Water EDR. For example, VIIRS short-wave infrared radiances are sensitive to surface parameters and less sensitive to water vapor absorption. Longwave VIIRS channels are, in contrast, sensitive to temperature and water vapor conditions. These two distinct measurement characteristics can provide a unique opportunity for VIIRS to retrieve precipitable water with good performance and work toward higher performance using an enhanced VIIRS configuration. Raytheon's precipitable water retrieval strategies take advantage of all available infrared radiances to obtain the Precipitable Water EDR in a non-linear statistical regression approach.

Since Raytheon's infrared retrieval uses the same algorithm and same input VIIRS data for both day and night, the retrieval system is relatively simple and no significant day/night biases will occur. The solar reflectance from the cloud and ground surfaces is explicitly accounted for during the retrieval process via a solar zenith angle term. The daytime Precipitable Water EDR might have slightly better performance due to the fact that the solar reflectance provides additional information to complement the infrared thermal signal. It is expected that if the algorithm is capable of modeling the solar component signal accurately, the daytime precipitable water retrieval will outperform its nighttime counterpart. Sensitivity studies of day and night precipitable water retrievals will be presented in section 3.4.1.

The VIIRS Precipitable Water EDR will use spectral bands at 3.7 μm, 4.05 μm, 8.55 μm, 10.78 μm, and 12.01 μm for all retrievals.

2.3.1 Clear Conditions

Clear precipitable water retrievals are performed when the VIIRS Cloud Mask identifies a pixel as clear or probably clear. In this case, the retrievals are considered to cover the total column of precipitable water integrated from the top of the atmosphere to the surface, using ancillary surface pressure data. The Precipitable Water EDR is classified by temperature and humidity to improve performance. Sensitivity studies of clear retrievals are presented in section 3.4.1.

2.3.2 Cloudy Conditions

Cloudy precipitable water retrievals are performed when the VIIRS Cloud Mask EDR identifies a pixel as cloudy or probably cloudy. Cloudy precipitable water retrievals are considered to represent the total column of precipitable water from the top of the atmosphere to the top of the clouds. Sensitivity study of cloudy precipitable water will be presented in section 3.4.1.7.

3.0 ALGORITHM DESCRIPTION

3.1 PROCESSING OUTLINE

Figure 8 shows the top level software architecture for the Precipitable Water EDR.

A fast VIIRS infrared forward model is required to process the VIIRS data. In addition, historical radiosonde profiles, which have the measures of temperature, water vapor, and surface skin temperature information, are required. This processing is to build non-linear regression coefficients to account for the statistical relationship between simulated VIIRS infrared radiances and precipitable water and surface emissivity. All the scenario parameters, such as sun/sensor geometry, surface level, clear or cloud level, and day and night information are all essential information to be used in the analysis. Cloud mask input is required to classify clear or cloudy regression retrieval. All VIIRS baseline infrared channels from short-wave 3.7 micron to 12 micron are used along with the measurement noise estimates, forward model error, surface emissivity, aerosol absorption modeling and sub-cirrus cloud contamination.

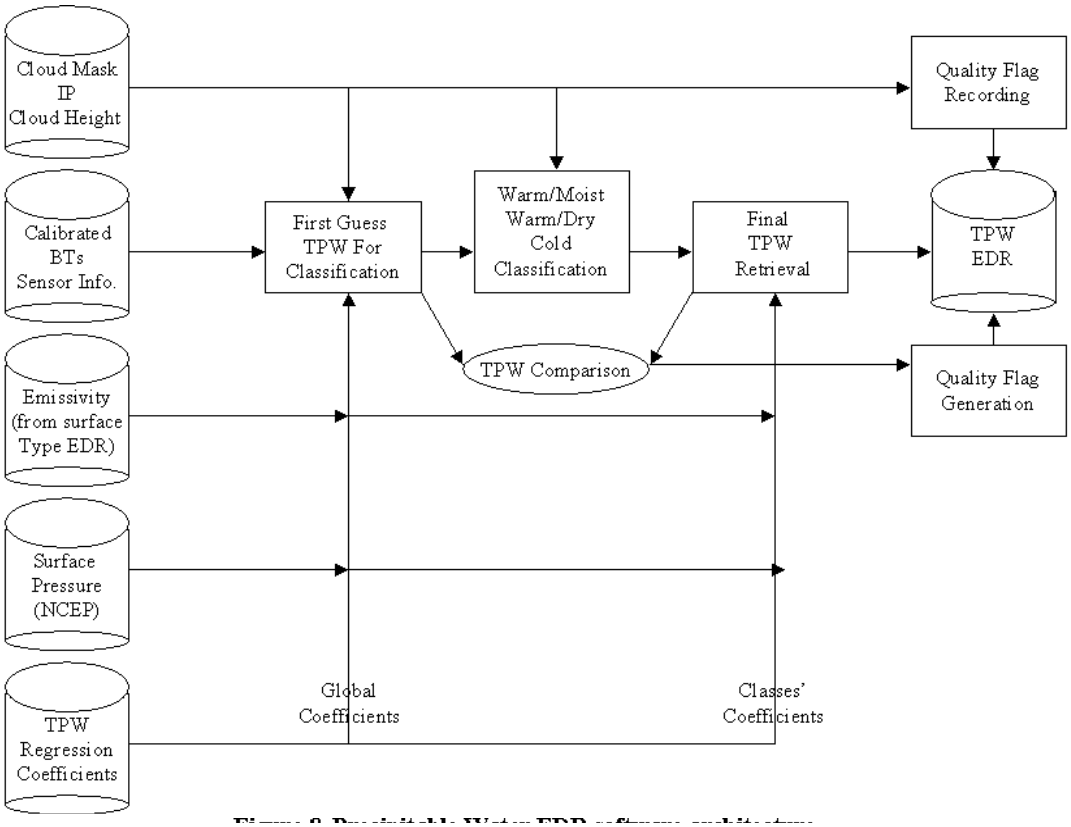

Figure 8. Precipitable Water EDR software architecture.

3.2 ALGORITHM INPUT

3.2.1 VIIRS Data

The TOA Calibrated Brightness Temperatures Sensor Data Record (SDR) is required for production of the VIIRS Precipitable Water EDR. This SDR includes the necessary solar and viewing zenith angle information, along with geolocation parameters. The VIIRS cloud mask is required to define a clear or cloudy Precipitable Water EDR retrieval. Pre-determined VIIRS surface emissivity information is also required to improve precipitable water retrieval at various surface conditions. This is derived using the most recent output of the VIIRS Surface Type EDR.

3.2.2 Non-VIIRS Data

Near real time (at most a few hours old) surface pressure is the essential non-VIIRS data input to the retrieval of precipitable water.

3.3 THEORETICAL DESCRIPTION OF RETRIEVALS

This section outlines the basic principles for obtaining precipitable water based on the non-linear relationship between precipitable water and VIIRS radiances, and it describes how the inverse problem can be physically and statistically formulated to accurately and efficiently deal with VIIRS precipitable water processing at pixel resolution.

3.3.1 Physics of the Problem

Top of atmosphere VIIRS radiances represent very complicated physical processes of radiative transfer, which are involved with multiple atmospheric effects. These effects include temperature and water vapor within the whole column path of the VIIRS IFOV, underlying clouds, surface boundaries, thermal reflections, cloud/aerosol scattering, and gaseous absorption. The non-unique and non-linear aspects of the precipitable water retrieval problem can be solved by a non-linear statistical regression approach.

3.3.1.1 Spectral Characteristics of Precipitable Water

The dependence of the differences between brightness temperatures in different VIIRS channels on the amount of precipitable water is shown in Figure 9 for both night and day. At night, brightness temperature differences between two VIIRS baseline shortwave channels display a nonlinear relationship with respect to the precipitable water amount. A linear increase in precipitable water does not correspondent to a linear increase in the two-channel difference. As matter of fact, it is interesting to see the opposite sign in the relationship between low and high amount of precipitable water. Differences between the 8.55 and 11 micron channels also exhibit a nonlinear relationship, however, unlike shortwave channel differences, the differences increase with the increase of the precipitable water amount. Longwave channel differences are much more linear with respect to the precipitable water amount. The differences between shortwave and longwave channels produce much more scattered distributions due to the greater surface emissivity variations between these two spectral regimes. During the day, due to the solar reflectance, the differences in the two shortwave channels are dramatically different than for the nighttime case, with a wider spread and higher nonlinearity with the amount of precipitable water. For other two-channel differences, no significant differences in behavior between day and

night are observed. As expected, differences between shortwave and longwave bands still exhibit broad scatter features.

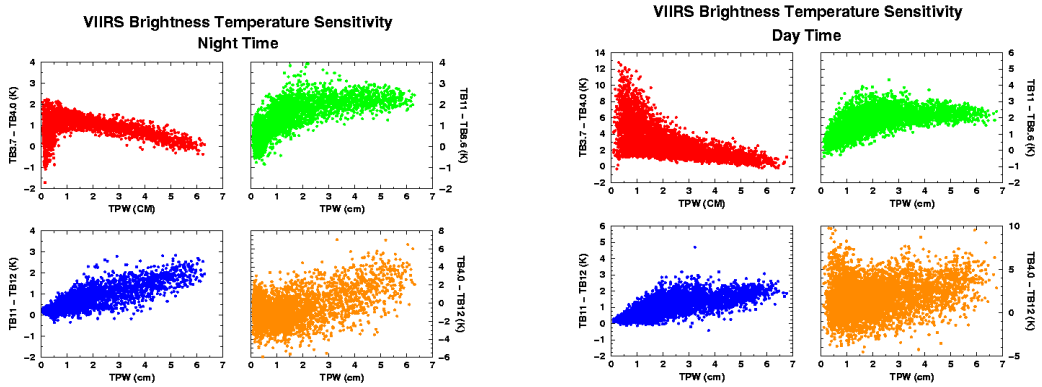

Figure 9. Scatter plots of VIIRS two-channel brightness temperature differences against precipitable water amount.

That precipitable water information exists in the VIIRS IR measurements is clearly demonstrated by the correlation plots between channel brightness temperatures and precipitable water, shown in Figure 10. In general, water vapor channels sensitive to certain layers of atmospheric water vapor provide much lower correlation to precipitable water when compared to channels with carbon dioxide (temperature) absorption information. It is very important to note that precipitable water information embedded in VIIRS IR measurements is strongly dependent not only on integrated column water vapor, but also on the temperature profile. For example, precipitable water correlation values range from 0.921 to 0.938 for carbon dioxide channels and from 0.388 to 0.861 for water vapor channels. It is clear from these correlation plots that VIIRS precipitable water retrievals can be incrementally improved if temperature-sensitive channels are incorporated into the instrument and precipitable water retrieval algorithm uses both water vapor and temperature channels simultaneously.

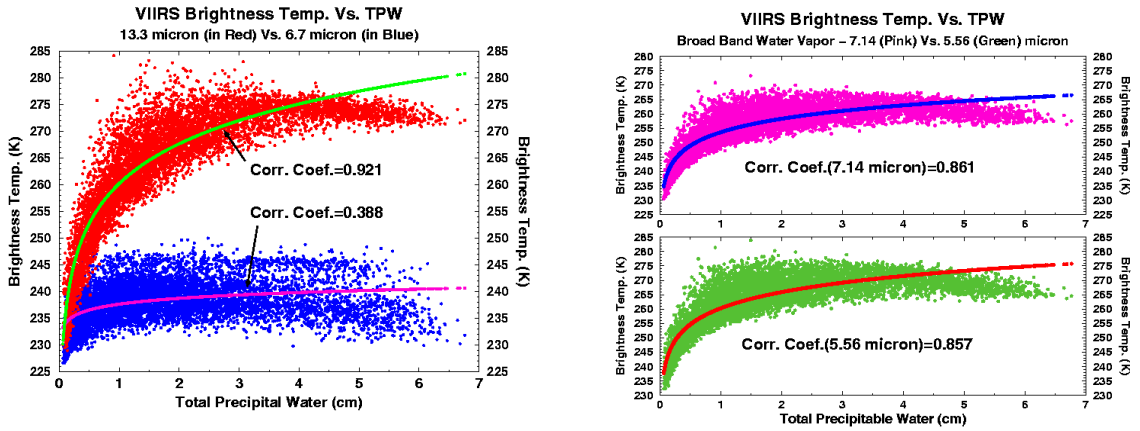

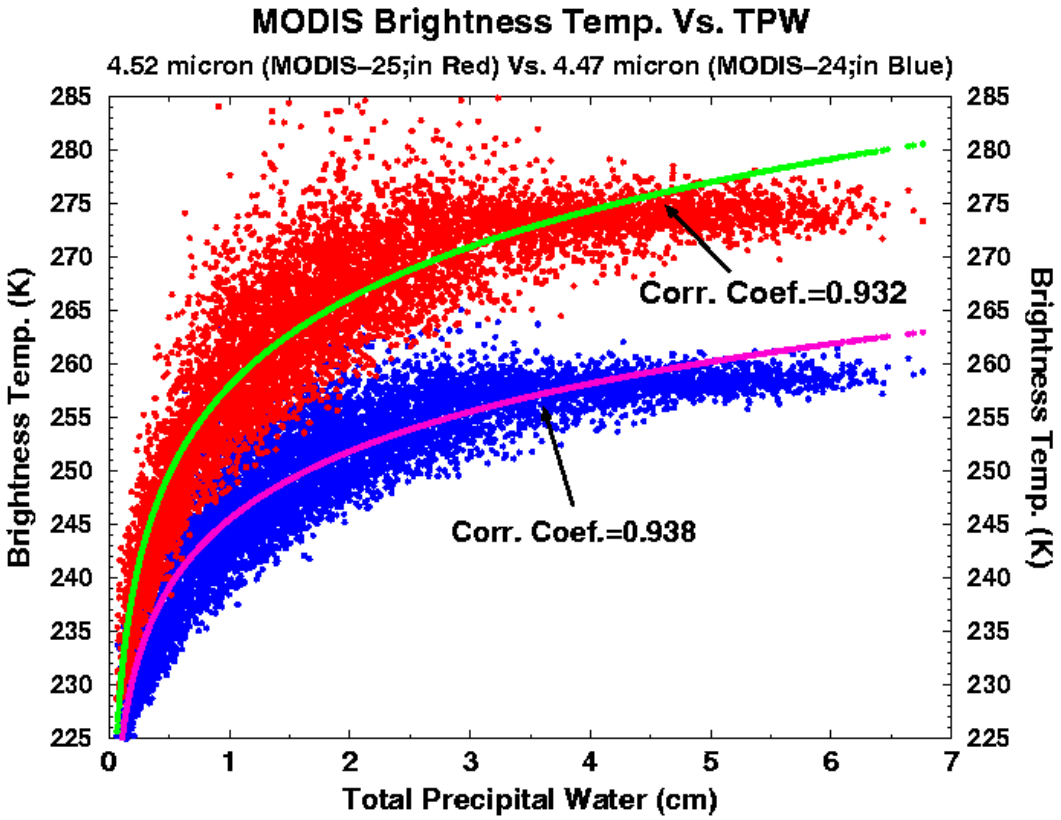

Figure 10. Correlation plots of IR temperature and water vapor channel brightness temperatures with precipitable water amount.

3.3.1.2 Historical Development of of Precipitable Water Products

Determination of the total column precipitable water is most directly obtained by integrating the moisture profile through the atmospheric column. However, several simpler approaches are also viable. They are briefly described below.

The split window method can be used to specify total water vapor concentration from clear sky $11\,um$ and $12\ um$ brightness temperature measurements. The water vapor is evaluated by observing the area of interest in both infrared window bands. In the atmospheric window regions, the absorption is weak so that

$$\tau_w = e^{-K_w u} \approx 1 - K_w u \tag{2}$$

where w denotes the window band, K is the absorption coefficient, and u is the total column water vapor path. What little absorption exists is due to water vapor, therefore, u is a measurement of precipitable water vapor. The measured radiance in the window region can be written from (1) if a blackbody surface is assumed

$$R_w = B_{sw}(1 - K_w u_s) + K_w \int_0^{u_s} B_w du \quad . \tag{3}$$

Defining an atmospheric mean Planck radiance

$$\overline{B}_w = \int_0^{u_s} B_w du \Big/ \int_0^{u_s} du \quad , \tag{4}$$

then

$$R_w = B_{sw}(1 - K_w u_s) + K_w u_s \overline{B}_w \quad . \tag{5}$$

Since B_{sw} is close to both R_w and B_w, a first order Taylor expansion about the surface skin temperature T_s allows us to linearize the RTE with respect to temperature, therefore

$$T_{bw} = T_s(1 - K_w u_s) + K_w u_s \overline{T}_w \quad , \tag{6}$$

where $\overline{T}_w$ is the mean atmospheric temperature corresponding to B_w. This implies that

$$u_s = [T_{bw} - T_s] \Big/ [K_w(\overline{T}_w - T_s)] \quad . \tag{7}$$

Obviously, the accuracy of the determination of the total water vapor concentration depends upon the contrast between the surface skin temperature and the effective temperature of the

atmosphere. In an isothermal situation, the total precipitable water vapor concentration is indeterminate. For two window spectral bands (11 and 12 μm) the split window approximation allows us to have

$$T_s = [K_{w2}T_{bw1} - K_{w1}T_{bw2}] \Big/ [K_{w2} - K_{w1}] \quad , \tag{8}$$

and if we express T_w as proportional to T_s

$$\overline{T}_w = a_w T_s \tag{9}$$

then a solution for u_s follows:

$$u_s = \frac{T_{bw2} - T_{bw1}}{(a_{w1} - 1)(K_{w2}T_{bw1} - K_{w1}T_{bw2})} = \frac{T_{bw2} - T_{bw1}}{b_1 T_{bw1} - b_2 T_{bw2}} \quad . \tag{10}$$

The coefficients b_1 and b_2 can be evaluated in a linear regression analysis from prescribed temperature and water vapor profile conditions coincident with in situ observation of u_s. The weakness of this method is due to the time and spatial variability of a_w and the insensitivity of a stable lower atmospheric state $T_{bw1} - T_{bw2}$ to the total precipitable water vapor concentration.

Another approach lies in the Split Window Variance Ratio, which starts from atmospheric windows with minimal moisture absorption

$$R_w = B_{sw}(1 - K_w u_s) + K_w u_s \overline{B}_w \quad .$$

Consider neighboring fields of view and assume that the air temperature is invariant. Then the gradients can be written

$$DR_w = DB_{sw}(1 - K_w u_s) \quad , \tag{11}$$

where D indicates the differences due to different surface skin temperature in the two FOVs. Convert to brightness temperatures with a Taylor expansion with respect to one of the surface skin temperatures, so that

$$[R_w(FOV1) - R_w(FOV2)] = [B_{sw}(FOV1) - B_{sw}(FOV2)](1 - K_w u_s) \quad , \tag{12}$$

$$[T_w(FOV1) - T_w(FOV2)] = [T_s(FOV1) - T_s(FOV2)](1 - K_w u_s) \quad . \tag{13}$$

Using the split windows can arrive an estimate for u_s in the following way. Write the ratio

$$\begin{aligned}\frac{1-K_{w1}u_s}{1-K_{w2}u_s} &= \frac{dR_{w1}dB_{sw2}}{dR_{w2}dB_{sw1}} \\ &= \frac{[R_{w1}(FOV1)-R_{w1}(FOV2)][B_{sw2}(FOV1)-B_{sw2}(FOV2)]}{[R_{w2}(FOV1)-R_{w2}(FOV2)][B_{sw1}(FOV1)-B_{sw1}(FOV2)]} \\ &= \frac{[T_{w1}(FOV1)-T_{w1}(FOV2)][T_s(FOV1)-T_s(FOV2)]}{[T_{w2}(FOV1)-T_{w2}(FOV2)][T_s(FOV1)-T_s(FOV2)]} \\ &= \frac{[T_{w1}(FOV1)-T_{w1}(FOV2)]}{[T_{w2}(FOV1)-T_{w2}(FOV2)]}\end{aligned} \tag{14}$$

The surface skin temperature cancels out, therefore

$$\frac{1-K_{w1}u_s}{1-K_{w2}u_s} = \frac{DT_{w1}}{DT_{w2}}, \tag{15}$$

or

$$u_s = (1-D_{12})/(K_{w1}-K_{w2}D_{12}), \tag{16}$$

where D_{12} represents the ratio of the deviations of the split window brightness temperatures. The deviation is often determined from the square root of the variance.

The assumption in this technique is that the difference in brightness temperatures from one FOV to the next is due only to the different surface skin temperatures. It is best applied to an instrument with relatively good spatial resolution, so that sufficient samples can be found in an area with small atmospheric variations and measurable surface variations in order to determine the variance of the brightness temperatures accurately. The technique was suggested by the work of Chesters et al (1983) and Kleepies and McMillin (1984); Jedlovec (1987) successfully applied it to aircraft data with 50 m spatial resolution to depict mesoscale moisture variations preceding thunderstorm development.

MODIS split window algorithm

The split window method can be used to specify total precipitable water from clear sky 11 µm and 12 µm brightness temperatures. In the atmospheric window channels, the absorption is week so that

$$\tau_i = \exp(-k_i w \sec\theta) \approx 1 - k_i w \sec\theta \tag{5}$$

Where I denotes the channel index, w is the total precipitable water, thus

$$d\tau_i = -k_i \sec\theta \, dw \tag{6}$$

In window channel, little absorption exists due to water vapor; therefore, w is a measure of column water vapor. The measured radiance in the thermal window region can be written from the Radiative Transfer Equation

$$\begin{aligned} R_i &= \varepsilon_i B_i(T_s)\tau_i + \int_0^{\tau} B_i(T(p))d\tau \\ &= \varepsilon_i B_i(T_s)(1 - k_i w \sec\theta) + k_i \sec\theta \int_0^{W} B_i(T(p))dw \end{aligned} \tag{7}$$

where W represents the total column water vapor or precipitable water. Defining an atmospheric mean Planck radiance

$$B_i(T_a) = \int_0^{W} B_i(T(p))dw \Big/ \int_0^{W} dw \tag{8}$$

$$R_i = \varepsilon_i B_i(T_s)(1 - k_i W \sec\theta) + k_i \sec\theta \, W B_i(T_a)$$

the Planck function can be expanded in a Taylor series about the brightness temperature Ti in the form of

$$R_i = B_i(T_i) = \frac{DB}{DT}\Big|_{T_i} \frac{B_i(T_i)}{\frac{DB}{DT}\Big|_{T_i}} = \frac{DB}{DT}\Big|_{T_i} L(T_i) \tag{9}$$

$$B_i(T_s) = B_i(T_i) + \frac{DB}{DT}\Big|_{T_i} (T_s - T_i) = \frac{DB}{DT}\Big|_{T_i} (T_s - T_i + L(T_i))$$

$$B_i(T_a) = B_i(T_i) + \frac{DB}{DT}\Big|_{T_i} (T_a - T_i) = \frac{DB}{DT}\Big|_{T_i} (T_a - T_i + L(T_i))$$

It can allow us to linearize the RTE with respect to temperature, so

$$L(T_i) = \varepsilon_i (1 - k_i w \sec\theta)(T_s - T_i + L(T_i)) + k_i w \sec\theta (T_a - T_i + L(T_i)) \tag{10}$$

Several approximations have been proposed for L (Ti). Price (1984) and Becker (1987) propose

$$L(T_i) = T_i / n_i \tag{11}$$

With this expression, total precipitable water can be expressed as

$$W = \frac{(C_{i1} T_i - \varepsilon_i T_s)\cos\theta}{k_i (T_a - \varepsilon_i T_s - C_{i2} T_i)} \tag{12}$$

Where

$$C_{i1} = \frac{1+(n_i-1)\varepsilon_i}{n_i},\ C_{i2} = \frac{(n_i-1)(1-\varepsilon_i)}{n_i}$$

$$\varepsilon_i \approx 1.0$$

For ocean, the emissivity at 11 and 12 μm

$$W = \frac{T_i - T_s}{k_i \sec\theta (T_a - T_s)} \tag{13}$$

Surface temperature Ts over ocean and for a specific surface type can be derived as (see VIIRS SST or LST ATBD)

$$Ts = T_1 - (T_2 - T_1)\,k_1/(k_2 - k_1) = \frac{k_2 T_1 - k_1 T_2}{(k_2 - k_1)} \tag{14}$$

And if we assume Ta as proportional to Ts

$$Ta = a_w Ts \tag{15}$$

Then a solution for W can be expressed as:

$$W = \frac{(T_2 - T_1)\cos\theta}{(a_w - 1)(k_2 T_1 - k_1 T_2)} = \frac{(T_2 - T_1)\cos\theta}{b_1 T_1 - b_2 T_2} \tag{16}$$

This is the MODIS precipitable water algorithm. As seen from our derivation, this algorithm can only be used over ocean. Otherwise, the assumption that Ta is proportional to Ts may lead to large errors.

3.3.2 Mathematical Description of VIIRS Algorithm

As shown in section 3.3.1.2 historical PW algorithm uses split window concept approach. Despite of many short and long –wave IR radiance channels are simultaneously available only two long-wave IR window channels are utilized. From figure 10 of 3.3.1.1 spectral characteristics of precipitable water, we demonstrate that many other IR channel exhibits excellent correlation with precipitable water. By taking advantages of VIIRS multiple IR radiance measurements, a simple regression approach can also applied to VIIRS data for precipitable water retrieval. This procedure is based on a single FOV's measurements or averaged measurements within FOVs. All infrared window spectral bands can be use in this procedure. For example, the precipitable water can be derived by

$$PW = a_0 + \sum_{i=1}^{NB} a_i Tb_i + \sum_{i=1}^{NB}\sum_{j=i}^{NB} c_{ij} Tb_i Tb_j + d_1 \sec\theta + d_2 p_s + d_3 \cos(\Phi) + d_4 Emis\,, \tag{17}$$

where Tb_i is the brightness temperature for i th spectral band, p_s is the surface pressure, θ and Φ are the satellite local zenith angle and solar zenith angle, respectively. Emis is surface

emissivity, to account for effects of different surface types. NB is the total number of VIIRS spectral bands used. a, c and d give the regression coefficients. Eq.(17) simply reflects the precipitable water information available from the VIIRs infrared window band measurements with additional surface and angle knowledge. The quadratic term is indicative of the nonlinear relationship in the regression between precipitable water and VIIRS IR window spectral band radiances.

3.3.3 Archived Algorithm Output

Precipitable water retrieval outputs include geo-location, precipitable water values, and quality flags indicating which class of retrieval is performed and whether the unclassified and classified precipitable water difference is reasonably small. The output is retained within the VIIRS processing stream for use by other algorithms, such as Surface Reflectance.

3.3.4 Variance and Uncertainty Estimates

Table 3 lists the requirements specified by the Integrated Program Office (IPO) for the Precipitable Water EDR.

Table 3. VIIRS SRD prescribed requirements for the Precipitable Water EDR.

SRD Parameter No.	Parameter	Threshold	Objective
V40.7.12-1	a. Horizontal Cell Size at Nadir	1 km (TBR)	1 km
V40.7.12-2	b. Horizontal reporting interval	(TBD)	(TBD)
V40.7.12-3	c. Horizontal coverage	Global	Global
V40.7.12-4	d. Measurement range	0 – 75 mm	0 – 100 mm
V40.7.12-5	e. Measurement Uncertainty	(TBD)	(TBD)
V40.7.12-6	f. Mapping Uncertainty	3 km	0.1 km
	g. Maximum local average revisit time	6 hrs	3 hrs
	h. Maximum local refresh	(TBD)	(TBD)
V40.7.12-7	i. Minimum swath width (all other EDR thresholds met)	3000 km (TBR)	(TBD)

Note that the key performance metric, measurement uncertainty, is TBD. MODIS data will allow a new level of performance in precipitable water retrievals, however this level is difficult to pin down without real application of the MODIS algorithms to real data.

3.4 ALGORITHM SENSITIVITY STUDIES

The VIIRS precipitable water non-linear regression retrieval sensitivity was studied using the simulation procedure described below. The precipitable water accuracy and precision were calculated from several components of uncertainty, including measurement error, forward model error, temperature and water vapor profile uncertainties, surface emissivity and reflectivity uncertainty, cloud height uncertainty, sub-visible cirrus cloud contamination, and aerosol contamination. Improvement due to the inclusion of an additional, temperature-sensitive, carbon dioxide spectral band is also studied.

3.4.1 Description of Simulations

In order to derive the regression coefficients, VIIRS infrared window band radiances calculated are generated from 7544 global radiosonde profiles. These radiosonde profiles contain atmospheric temperature, moisture and ozone. A fast atmospheric transmittance model, Pressure Layer Optical Depth (PLOD) (Hannon, et al. 1996), is used for the radiative transfer calculations. PLOD uses 42 vertical pressure level coordinates ranging from 0.1 to 1050 hPa. The VIIRS instrument noise plus an assumed 0.2K forward model error is added into the simulated VIIRS infrared band radiance. The regression coefficients are generated based on the following two configurations:

1) Global Regression Coefficients

90% of the 7544 global profiles (dependent samples) are used to generate the regression coefficients; these coefficients are then applied to the remaining 10% of the simulated VIIRS spectral measurements (independent samples) to get the precipitable water retrieval. The precision expressed in terms of total column precipitable water error in percent is defined as

$$\Pr ecision = 100\% \times \sqrt{\frac{1}{NS}\sum_{j=1}^{NS}\left(\frac{PW_j^{true} - PW_j^{rtv}}{PW_j^{true}}\right)^2}, \qquad (18)$$

where PW^{true} and PW^{rtv} are "true" precipitable water and regression derived retrieval values respectively, calculated using Eq.(17), and NS is the number of independent samples.

2) Classified Regression Coefficients

In this configuration, 90% of 7544 global profiles are classified as “warm and moist”, “warm and dry” and “cold”. The regression coefficients are generated for each class. These coefficients are based on the classification using 11 micron band brightness temperature and unclassified global retrieved precipitable water. After successful classification, the classified coefficients are then applied to the remaining 10% of the profiles for precipitable water retrieval analysis. There are two steps in the classification. In the first step, the 11 micron band brightness temperature is used to classify into a warm or cold class. If the brightness temperature of the 11 micron band is warmer than 282 K, then it is placed in the warm class. A first guess global precipitable water retrieval is then performed using global coefficients. This first guess is used in the second step to further classify the pixel as dry or moist, but only if it has first been classified as warm. For the cold class (brightness temperature colder than 282 K), no further classification will be made. As a result, there are three classes, namely “warm and dry”, “warm and moist”, and “cold”. Including the global case, there are then four sets of precipitable water regression retrieval coefficients that should be updated every month using the past 13 months of global radiosonde profiles. To minimize discontinuities and the effects of misclassification, some overlap between classes is established.

3.4.1.1 Measurement noise sensitivity

VIIRS precipitable water retrieval sensitivity towards measurement noise is demonstrated in Figure 11. A noise factor of 1 means precipitable water is derived from the specification for

VIIRS sensor noise. A noise factor of 0.2 essentially represents very high precision VIIRS measurements and noise factor of 2 implies the noise has been increased two times. Precipitable water retrieval precision, expressed in terms of percent error, is shown to be a nearly linear function of noise factor, however the relationship is not overly strong. Unclassified and classified global precipitable water retrieval were also investigated and found to have similar sensitivity to the measurement noise.

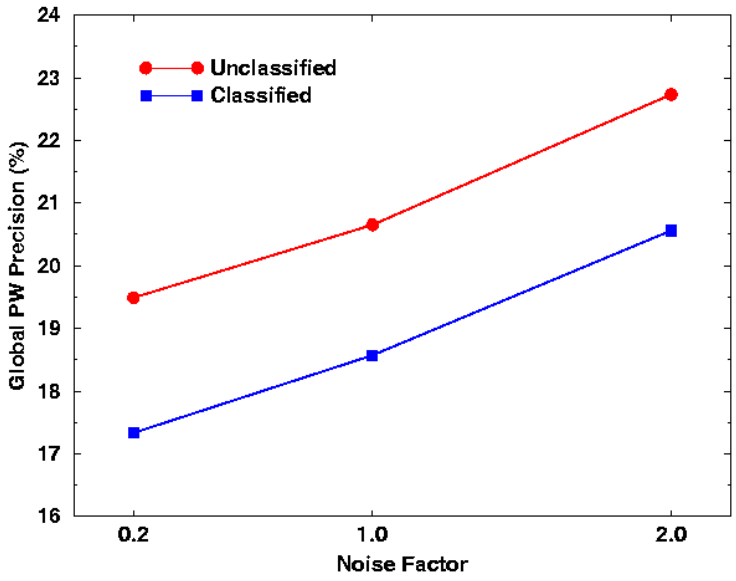

Figure 11. Precipitable water retrieval sensitivity to sensor noise (noise factor of 1 is equal to VIIRS spec).

3.4.1.2 Carbon dioxide band sensitivity

As discussed in section 3.3.1.1, carbon dioxide channels are highly correlated with precipitable water and would provide additional precipitable water retrieval information on top of baseline VIIRS measurement capability. Figure 12 demonstrates global precipitable water retrievals using the baseline VIIRS bands combined with other possible bands to enhance performance. A carbon dioxide band can indeed provide additional precipitable water information, and a 4.52 micron band seems to provide the best retrieval precision when compared with baseline performance.

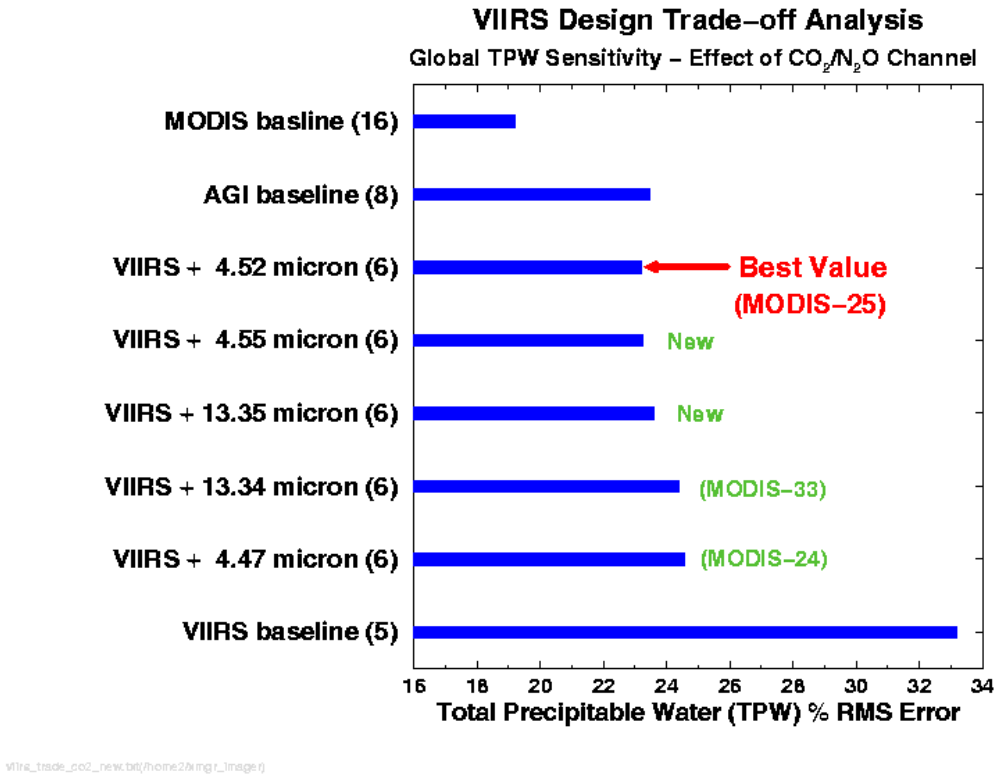

Figure 12. Trade study on optimal band combinations for precipitable water retrieval. "VIIRS" means the VIIRS baseline.

Figure 13 also demonstrates the enhancement of precipitable water retrieval precision due to the addition of carbon dioxide 4.5 micron band for four different region scenes simulated besides the global scene shown in the previous figure. These four scenes were simulated from September 13/14 of 1998 CAMEX-3 NAST-I retrieved sounding profile and NAST-I PW was used as true to assess the VIIRS PW precision for baseline and baseline with 4.5 micron band instrument measurement configuration. For the present, the VIIRS baseline will remain in its current configuration, without the addition of the 4.5 micron band. This decision emerged from a cost versus performance analysis conducted by the algorithm and sensor teams. Room for spare bands does exist, however, and the issue may be revisited in the future. It should be noted that the present VIIRS baseline performs quite well with regard to precipitable water retrievals.

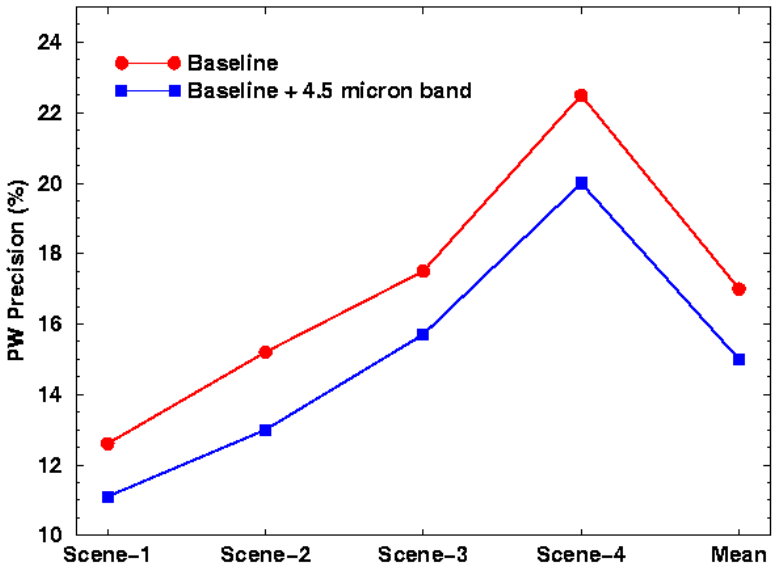

Figure 13. Utility of adding a 4.5 micron band to the VIIRS baseline for precipitable water retrievals.

3.4.1.3 Land and Ocean surface sensitivity

Figure 14 shows how surface emissivity variations can affect brightness temperature in the five baseline bands used by the precipitable water algorithm. Over oceans, a 0.5% emissivity variation is typical, while over land a few percent in emissivity variation is possible. These results indicate why an emissivity term is necessary in the regression equation.

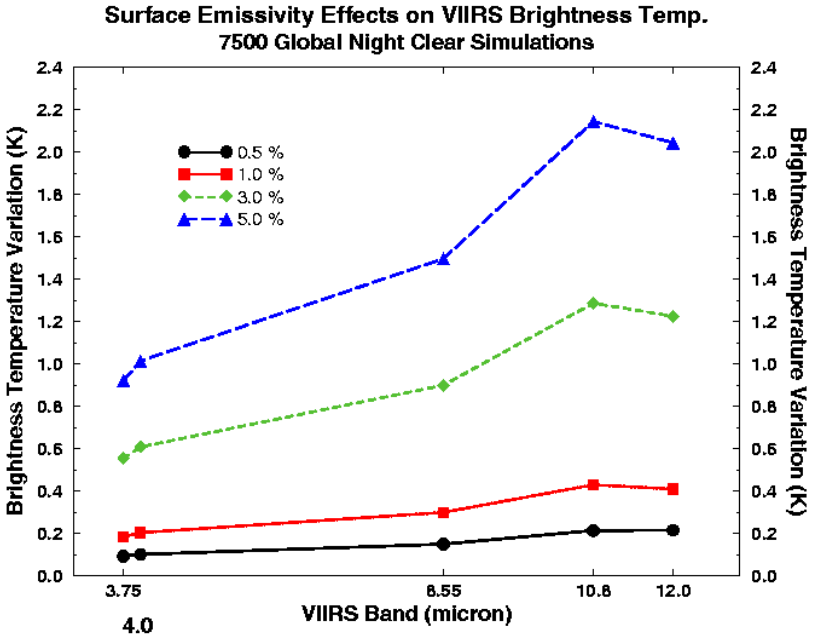

Figure 14. VIIRS brightness temperature variations due to changes in surface emissivity.

The resulting surface emissivity uncertainty can degrade the precipitable water retrieval precision if its effects are not accounted for. Figure 15 shows the precipitable water retrieval uncertainty over land and ocean surfaces, using different combinations of bands. Over land surfaces, a 3% surface emissivity uncertainty is assumed. Over oceans, 0.5% emissivity error is assumed. Obviously, better knowledge of emissivity or smaller surface emissivity variations will result in a more accurate precipitable water retrieval.

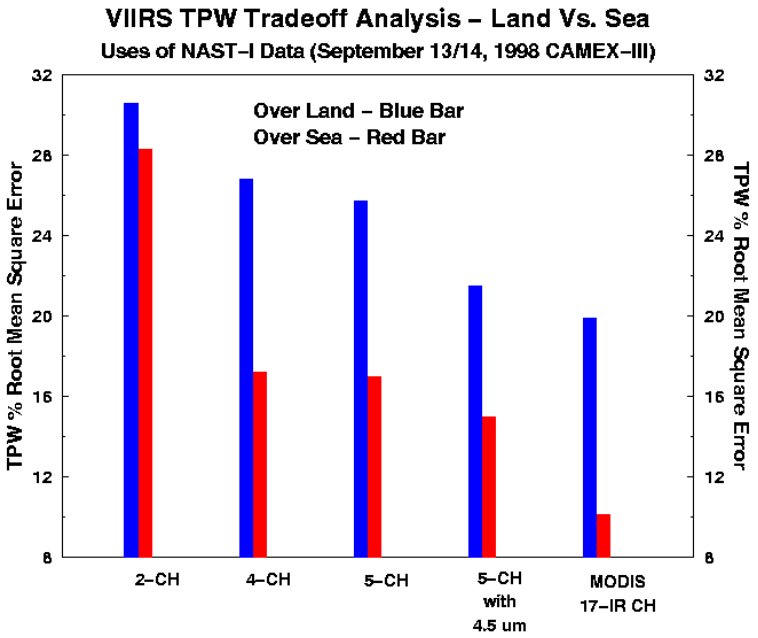

Figure 15. Precipitable Water EDR algorithm performance for land and ocean surfaces.

3.4.1.4 Aerosol contamination sensitivity

Two types of aerosol, namely maritime and continental, were modeled in the precipitable water retrieval sensitivity studies. Figure 16 demonstrates the brightness temperature depression due to aerosol absorption.

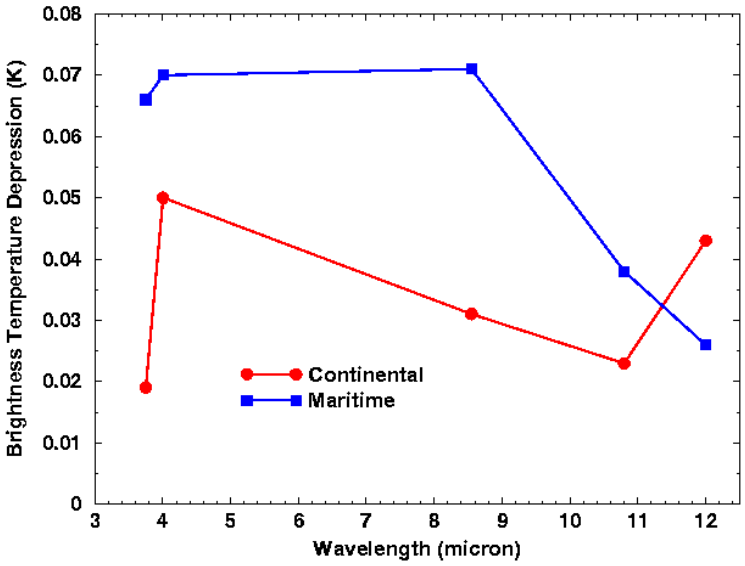

Figure 16. Brightness temperature depression due to absorption by continental or maritime aerosol.

Figure 17 shows that both types of aerosol can degrade the precipitable water retrieval, but only very slightly for typical aerosol optical thickness. Aerosol effects on unclassified and classified precipitable water retrievals are almost the same. Aerosol detection and correction prior to PW retrieval can improve PW performance, during phase II this kind of analysis will be conducted and the end results will be presented in version 5 ATBD.

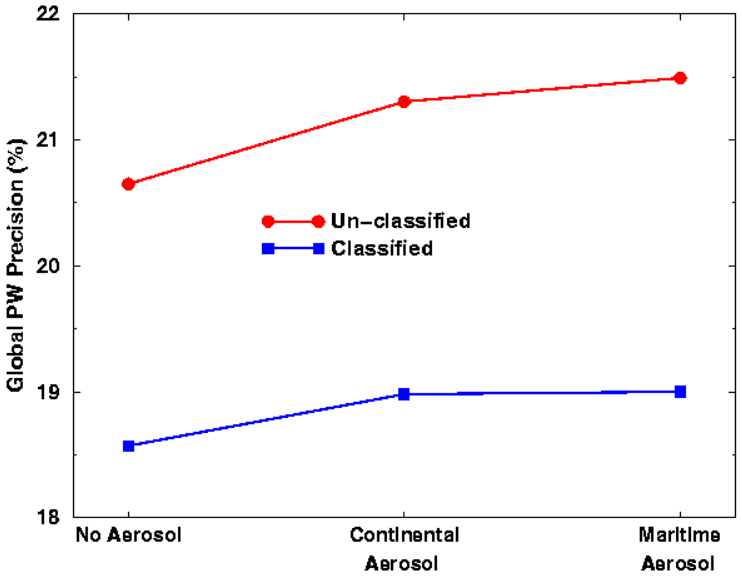

Figure 17. Aerosol effects on precipitable water retrieval precision. Red line shows errors when air mass is unclassified; blue line shows results when classification is done.

3.4.1.5 Sub-visible cirrus cloud contamination sensitivity

Sub-visible cirrus cloud is defined by an optical thickness not greater than 0.05. Three optical thicknesses—0.01, 0.02, and 0.05—were investigated. Very thin cirrus with an optical thickness of 0.01 attenuates VIIRS IR measurements by approximately 0.5 K, but with 0.05 optical thickness a brightness temperature depression of up to 2.5 K for some bands is possible. Figure 18 shows the root mean square difference affected by the presence of thin cirrus. The cirrus cloud attenuation is systematic, and the bias can be removed if these sub-visible cirrus clouds can be detected or if a correction is made. Sub-visible cirrus detection and correction prior to PW retrieval can improve PW performance, during phase II this kind of analysis will be conducted and the end results will be presented in version 5 ATBD.

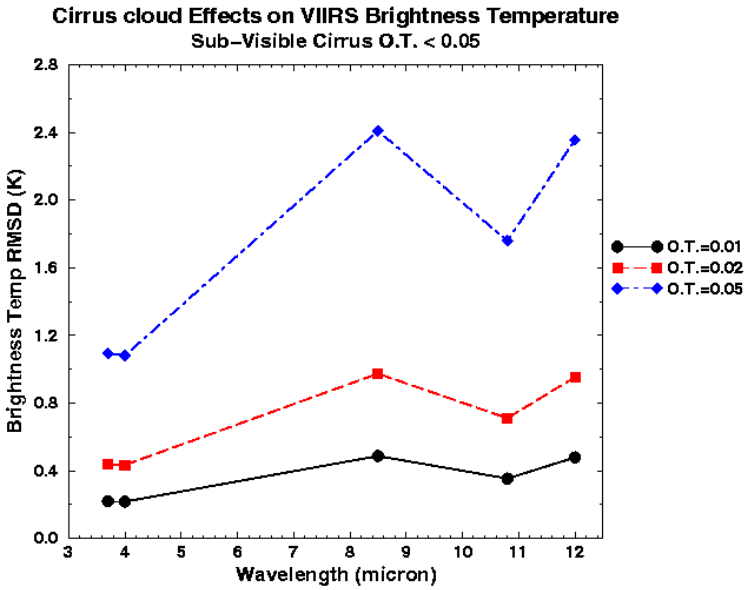

Figure 18. Effects of thin cirrus contamination on TOA brightness temperature in five VIIRS bands.

Figure 19 shows the consequences of thin cirrus contamination, both for no correction and a perfect correction. When the cirrus cloud is very thin, the precipitable water retrievals have very small differences regardless of knowledge of cloud. When sub-visible cirrus grows thicker, the contamination can degrade precipitable water up to 3 to 4 percent. Based on these results, a thin cirrus correction routine will be incorporated into the precipitable water algorithm, based on the same principles as the correction routine used for Sea Surface Temperature, and described in the Sea Surface Temperature ATBD.

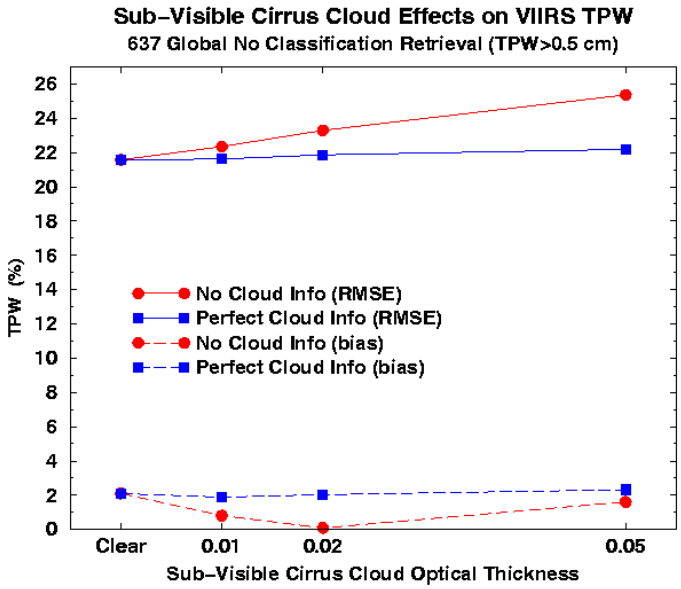

Figure 19. Precipitable water uncertainty and accuracy performance due to cirrus contamination.

3.4.1.6 Classification benefits

As described in sec. 3.4.1, one unclassified and three classified sets of global precipitable water retrieval regression coefficients were derived to perform global precipitable water retrieval. In this section the precipitable water retrieval performance is compared between unclassified and classified approaches. Figure 20 displays the scatter plot of these two approaches. In general, the unclassified approach shows larger scatter than classified approach for a wide range of precipitable water values. Other finer classification scheme can further improved PW performance. The refined classification scheme will be implemented during phase II and the end results will be presented in version 5 ATBD.

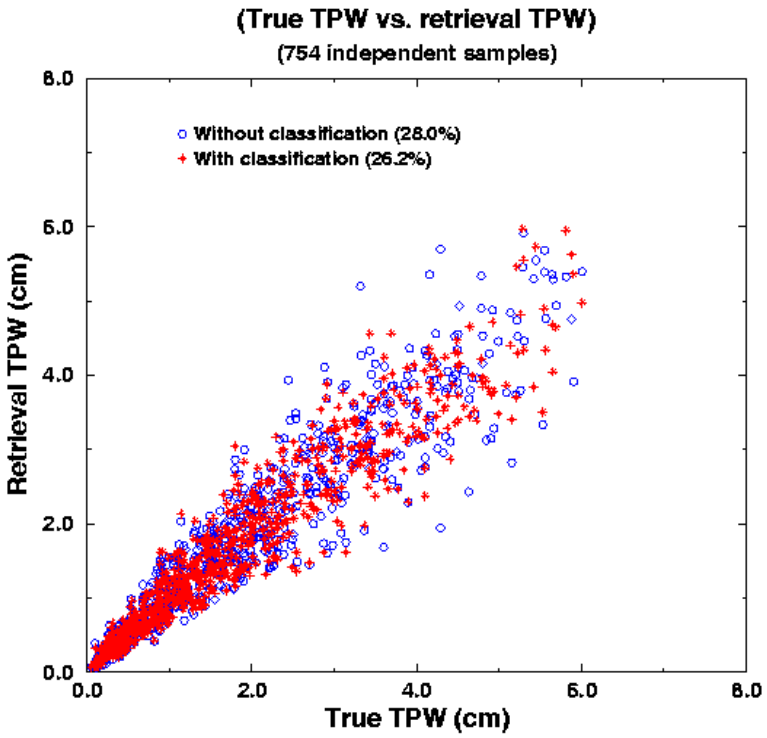

Figure 20. Scatter plot of retrieved versus true precipitable water; circles are for unclassified case, triangles are for classified case.

Table 4 details the precipitable water retrieval performance for unclassified and classified sub-classes using either four or five baseline IR bands, for the full range of precipitable water values. Significant improvement can be seen when using the classification process.

Table 4. Precipitable water uncertainty results for global retrievals using classified and unclassified approaches. "4-CH" refers to application of algorithm without the 8.55 micron band.

Class		Global	Global Classified	Warm	Cold	Warm & Moist	Warm & Dry
No. of Retrievals		754	754	392	444	225	331
Precipitable Water Uncertainty (%)	4 CH.	28.13	26.57	22.74	25.57	14.84	20.78
	5 CH.	27.99	25.99	22.62	25.37	14.52	19.54

Table 5 further illustrates the precipitable water retrieval performance comparisons between unclassified and classified approaches. Performance is reported as percent error for precipitable water greater than 10 mm and in millimeters for precipitable water less than 10 mm. Classified global performance is uniformly better than performance for the unclassified approach.

Table 5. Stratified precipitable water performance for clear conditions.

Precipitable Water Uncertainty	Global Unclassified		Global Classified	
Range	%	Mm	%	mm
precipitable water > 5 mm	22.86	5.24	21.58	4.19
precipitable water > 10 mm	20.65	5.73	18.57	4.55
precipitable water = 0-5 mm	43.62	1.07	40.04	1.05
precipitable water = 0 – 10 mm	35.31	1.85	35.0	1.80

3.4.1.7 Cloudy retrievals

Under cloudy conditions, the Precipitable Water EDR is defined as the integrated total column water vapor down to the cloud level only. In this analysis, cloud height knowledge is assumed to have 40 mb of uncertainty for high and mid level clouds and 100 mb for low level clouds. Retrieved precipitable water uncertainty is shown as a function of cloud fraction and cloud level in Table 6, Table 7, and Table 8. High, mid and low level clouds are represented by 300, 500 and 800 mb cloud top pressures, respectively. Retrievals over fractional cloud cover are more difficult than for complete or nonexistent cloud cover. Percent error becomes much larger for the dryer retrievals typically seen over clouds. Since cloud top height is a necessary input for cloudy PW process. We'll conduct further study to optimize the use of cloud top height information.

Table 6. Precipitable water performance for high clouds, stratified by cloud fraction.

High Cloud (Cloud Pressure = 300 mb)							
Cloud Fraction	0.0	0.2	0.4	0.6	0.8	0.9	1.00
Baseline (g/kg) X 10-3	18.5	25.7	24.2	22.2	21.4	23.0	25.5
Baseline+4.57 (g/kg) X 10-3	15.6	24.4	27.4	28.3	27.5	27.5	26.3

Table 7. Precipitable water performance for middle clouds, stratified by cloud fraction.

Middle Cloud (Cloud Pressure = 500 mb)							
Cloud Fraction	0.0	0.2	0.4	0.6	0.8	0.9	1.00
Baseline (g/kg) X 10^{-2}	7.7	9.3	9.1	8.3	7.7	8.0	8.4
Baseline+4.57 (g/kg) X 10^{-2}	4.4	6.6	7.1	7.7	7.3	7.2	7.4

Table 8. Precipitable water performance for low clouds, stratified by cloud fraction.

Low Cloud (Cloud Pressure = 800 mb)							
Cloud Fraction	0.0	0.2	0.4	0.6	0.8	0.9	1.00
Baseline (g/kg) X 10^{-1}	2.4	3.1	2.8	2.4	2.1	2.0	1.97
Baseline+4.57 (g/kg) X 10^{-1}	1.7	2.3	2.4	2.2	2.0	1.8	1.76

3.5 PRACTICAL CONSIDERATIONS

3.5.1 Numerical Computation Considerations

Paragraph SRDV3.2.1.5.4-1 of the VIIRS SRD states the following:

> "The scientific SDR and EDR algorithms delivered by the VIIRS contractor shall be convertible into operational code that is compatible with a 20 minute maximum processing time at either the DoD Centrals or DoD field terminals for the conversion of all pertinent RDRs into all required EDRs for the site or terminal, including those based wholly or in part on data from other sensor suites."

RDR here stands for Raw Data Record. This essentially means that any and all EDRs must be completely processed from VIIRS raw data, including calibration and georeferencing within 20 minutes from the time the raw data are available. This requirement is a strong reminder that VIIRS is an operational instrument.

The non-linear precipitable water regression requires little computer time to retrieve precipitable water, but it does require pre-computed offline retrieval coefficients. A monthly update of these coefficients is expected using the past 13 months of global radiosonde profiles. Near real time surface pressure information is also required.

3.5.2 Programming and Procedural Considerations

Research grade code has been delivered for the Precipitable Water EDR at the Preliminary Design Review (PDR). The algorithm itself is straightforward and easily implemented, and continued refinement will be applied in Phase II.

3.6 ALGORITHM VALIDATION

Pre-launch field experiment data sets emulating measurements of VIIRS and related in-situ data can provide best validation of the algorithm. Past and scheduled experiments such as CAMEX-II, CAMEX-III, SUCCESS, WINCE, WISC-T2000, SAFARI 2000, and MODIS data collected onboard Terra can be used to validate the algorithm by comparing retrieved precipitable water from MAS and MODIS data with regular radiosonde and special in-situ precipitable water observations.

4.0 ASSUMPTIONS AND LIMITATIONS

4.1 ASSUMPTIONS

The following assumptions are made with respect to the retrievals described in this document:

The fast infrared forward model calculation under cloudy conditions assumes blackbody behavior by the clouds. No rigorous quality checking was applied to precipitable water retrievals, except that precipitable water was not allowed to be negative. For classified precipitable water retrievals, if there exists a significant difference between the first guess and the final classified retrieval, a quality flag will be raised. Assumptions about the aerosol and thin cirrus cloud absorption correction only for the first order effects only. Detection and correction schemes are yet to be developed and implemented. Next version ATBD document will reflect all necessary adjustments on these assumptions.

4.2 LIMITATIONS

The following limitations apply to the at-launch retrievals of described in this document:

Solar reflectivity and surface emissivity are modeled theoretically, and further validation of the emissivity and reflectivity model is needed. The fast infrared forward model is modeled in a broad band sense. Validation of accuracy of this model needs to be conducted. Limitations of the analysis and results shown in this current version of ATBD is theoretical oriented. Further extensive validation of real VIIRS like measurement PW EDR retrieval need to be demonstrated.

5.0 REFERENCES

Chesters, D., L. W. Uccellini, and W. D. Robinson, 1983: Low-level water vapor fields from the VISSR Atmospheric Sounder (VAS) "split window" channels. J. *Clim. Appl. Met.*, 22, 725-743.

Hannon, S., L. L. Strow, and W. W. McMillan, 1996: Atmospheric Infrared Fast Transmittance Models: A comparison of Two Approaches. *Proceedings of SPIE Conference 2830*, Optical Spectroscopic Techniques and Instrumentation for Atmospheric and Space Research II.

IPO (2000). Visible/Infrared Imager/Radiometer Suite (VIIRS) Sensor Requirements Document (SRD) for National Polar-Orbiting Operational Environmental Satellite System (NPOESS) spacecraft and sensors, Rev. 2b/c. Prepared by Assoc. Directorate for Acquisition, NPOESS Integrated Program Office, Silver Spring, MD.

Jedlovec, G. J., 1987: Determination of atmospheric moisture structure from high resolution MAMS radiance data. Ph.D. Thesis, University of Wisconsin-Madison.

Kleespies, T. J., and L. M. McMillin, 1984: Physical retrieval of precipitable water using split window technique. Preprints Conf. On Satellite Meteorology/Remote Sensing and Applications, AMS, Boston, 55-57.

Planet, W.G. (ed.), (1988). Data extraction and calibration of TIROS-N/NOAA radiometers. NOAA Technical Memorandum NESS 107 – Rev. 1, Oct. 1988. 130 pp.